

STRUCTURAL STUDIES AND EVALUATION OF INHIBITORS OF *Mycobacterium*
tuberculosis H37Rv SHIKIMATE DEHYDROGENASE (MtSDH)

A Thesis

by

MALLIKARJUN LALGONDAR

Submitted to the Office of Graduate and Professional Studies of
Texas A&M University
in partial fulfillment of the requirements for the degree of

MASTER OF SCIENCE

Chair of Committee,	James C. Sacchettini
Committee Members,	David P. Barondeau
	Mary Bryk

Head of Department,	Gregory D. Reinhart
---------------------	---------------------

May 2014

Major Subject: Biochemistry

Copyright 2014 Mallikarjun Lalgondar

ABSTRACT

Shikimate dehydrogenase (SDH) is a reversible enzyme catalyzing the reduction of 3-dehydroshikimate (3DHS) to shikimate (SKM) utilizing NADPH cofactor in the shikimate pathway, a central route for biosynthesis of aromatic amino acids, folates and ubiquinones in microorganisms, plants and parasites, which renders the enzymes of this essential pathway as attractive targets for developing antimicrobials, herbicides and antiparasitic agents. In this study, the crystal structure of *Mycobacterium tuberculosis* SDH (MtSDH) was determined in the apo-form and in complex with a ligand, SKM. The overall structure of MtSDH contains two structural domains with α/β architecture. The N-terminal substrate binding domain and C-terminal cofactor binding domain are interconnected by two helices forming an active site groove where catalysis occurs. In MtSDH, a series of helices connecting $\beta 10$ and $\beta 11$ strands replace a long loop found in other known SDH structures and this region may undergo structural changes upon cofactor binding. NADP⁺ was modeled reliably in the cofactor binding site to gain insight into specific interactions. The analysis reveals that NADP(H) binds in *anti* conformation and in addition to residues in “basic patch”, Ser125 within the glycine rich loop may interact with the 2'-phosphate of adenine ribose and form a novel cofactor binding microenvironment in SDH family of enzymes. Biochemically, five inhibitors identified previously from a high-throughput enzyme assay screen were evaluated. The IC₅₀ values of these compounds range from 2.8-4.6 μ M. Further investigation indicates that these compounds display non-competitive or mixed inhibition mode with both

substrate and cofactor. This study is expected to provide better understanding of MtSDH structural features and a framework for rational design of inhibitors based on initially characterized compounds.

ACKNOWLEDGEMENTS

I would like to thank my committee chair, Dr. James C. Sacchettini, and my committee members, Dr. David P. Barondeau and Dr. Mary Bryk, for their guidance and support throughout the course of my research work.

I am thankful to my friends, colleagues and the departmental staff and faculty for providing a profound experience at Texas A&M University.

Finally, thanks to my parents, wife and children for their encouragement, patience and love.

NOMENCLATURE

3DHS	3-dehydroshikimate
A	Alanine
Ala	Alanine
Asn	Asparagine
Asp	Aspartate
D	Aspartate
DMSO	Dimethyl sulfoxide
DSF	Differential scanning fluorimetry
DTT	Dithiothreitol
G	Glycine
Gln	Glutamine
Gly	Glycine
I	Isoleucine
Ile	Isoleucine
IPTG	Isopropyl- β -D-1-thio-galactopyranoside
K	Lysine
L	Leucine
Leu	Leucine
Lys	Lysine
M	Methionine

Met	Methionine
Mtb	Mycobacterium tuberculosis
N	Asparagine
NAD ⁺	Nicotinamide adenine dinucleotide
NADP ⁺	Nicotinamide adenine dinucleotide phosphate
NADPH	Nicotinamide adenine dinucleotide phosphate reduced
PCR	Polymerase chain reaction
PMSF	Phenylmethanesulfonyl fluoride
Q	Glutamine
Rmsd	Root mean square deviation
S	Serine
SAD	Single-wavelength anomalous diffraction
SDH	Shikimate dehydrogenase
Ser	Serine
SKM	Shikimate
TB	Tuberculosis
Tyr	Tyrosine
Val	Valine
Y	Tyrosine

TABLE OF CONTENTS

	Page
ABSTRACT	ii
ACKNOWLEDGEMENTS	iv
NOMENCLATURE	v
TABLE OF CONTENTS	vii
LIST OF FIGURES	viii
LIST OF TABLES	ix
1. INTRODUCTION	1
2. EXPERIMENTAL PROCEDURES	6
2.1 Cloning, protein over-expression and purification	6
2.2 Crystallization, data collection and processing	7
2.3 Structure solution and model refinement	9
2.4 Differential scanning fluorimetry	11
2.5 MtSDH enzymatic assays	11
3. RESULTS AND DISCUSSION	13
3.1 Structure determination of MtSDH	13
3.2 Overall structure of apo-MtSDH and binary complex with shikimate	14
3.3 Conformational flexibility of MtSDH	17
3.4 Analysis of the substrate-binding domain	19
3.5 Analysis of the cofactor-binding domain	21
3.6 Mode of substrate and cofactor-binding, recognition and catalysis	24
3.7 MtSDH thermal denaturation profiles with substrates and inhibitors	27
3.8 MtSDH initial velocity studies and evaluation of inhibitors	30
4. SUMMARY AND CONCLUSION	40
REFERENCES	43

LIST OF FIGURES

	Page
Figure 1. Reaction catalyzed by shikimate dehydrogenase (SDH).	2
Figure 2. Overall structure of MtSDH.....	16
Figure 3. Structural elements of MtSDH closed conformation.....	18
Figure 4. Shikimate and its interactions with MtSDH.	20
Figure 5. Interactions of MtSDH with shikimate and NADP ⁺	24
Figure 6. Thermal denaturation profile of MtSDH.	29
Figure 7. Dose-dependent inhibition of MtSDH.	31
Figure 8. Inhibition of MtSDH toward 3DHS with increasing concentration of compounds.....	35
Figure 9. Inhibition of MtSDH toward NADPH with increasing concentration of compounds.....	36

LIST OF TABLES

	Page
Table 1. Selected inhibitors of MtSDH.....	5
Table 2. Summary of diffraction data and refinement statistics.....	10
Table 3. Transition melting point, T_m of MtSDH..	28
Table 4. MtSDH inhibition kinetics toward 3DHS titration.	33
Table 5. MtSDH inhibition kinetics toward NADPH titration.....	34
Table 6. Summary of MtSDH inhibition.....	37

1. INTRODUCTION

Mycobacterium tuberculosis (*Mtb*) is the main causative agent of tuberculosis (TB) disease resulting in loss of many human lives. It has been one of the most successful human pathogens, evident from the fact that one-third of the human population is estimated to be currently infected with latent TB (1). Each year 8 million new cases of *Mtb* infection are reported, of which 5-10% of the patients will potentially develop active TB in their lifetime. TB continues to claim more than 1.5 million lives annually and is a major concern for human health, because it is a contagious airborne disease. In 1940s and 50s, streptomycin, isoniazid, rifampicin, ethambutol and pyrazinamide were introduced as front line drugs and to date continue to be used effectively as primary anti-tubercular drugs. However, the long duration of the drug regimen has in some cases resulted in incomplete therapy. Consequently, the evolution of single-drug resistant (SDR), multi-drug resistant (MDR) and extensive-drug resistant (XDR) (2) strains of *Mtb* has exacerbated the problem. Therefore, there is an urgent need to develop new and effective drugs against *Mtb* to pre-empt the re-emergence of pandemic TB. One of the modern approaches to developing new drugs for diseases entails identification of suitable molecular targets. The availability of complete genome sequence of *Mtb* (3) has led to identification, testing and validation of molecular targets/pathways for development of new anti-mycobacterial compounds.

The shikimate pathway plays a fundamental role by linking carbohydrate metabolism to the biosynthesis of aromatic compounds in bacteria, fungi, plants and

apicomplexan parasites (4, 5). The pathway begins with utilization of phosphoenolpyruvate and erythrose 4-phosphate through a series of seven enzymatic steps to yield chorismate, a critical precursor incorporated during biosynthesis of aromatic amino acids, folates and ubiquinones (4). The absence of this pathway in metazoans renders it an attractive target for inhibitor development with applications as anti-microbials, herbicides and anti-parasitic agents with low mammalian toxicity. The widely used broad spectrum herbicide glyphosate is known to inhibit 5-enolpyruvylshikimate-3-phosphate (EPSP) synthase (6, 7), sixth enzyme of the pathway, providing evidence that this pathway is validated for inhibitor development with practical utility. In *Mtb*, this pathway has been shown to be essential for cell viability, despite addition of supplements in relation to the pathway (8).

Shikimate dehydrogenase (SDH) is the fourth enzyme in the shikimate pathway and belongs to a family of NAD(P)H-dependant oxidoreductases (EC 1.1.1.25). The enzyme catalyzes the reversible reduction of 3-dehydroshikimate (3DHS) to shikimate (SKM) utilizing NADPH cofactor (Figure 1).

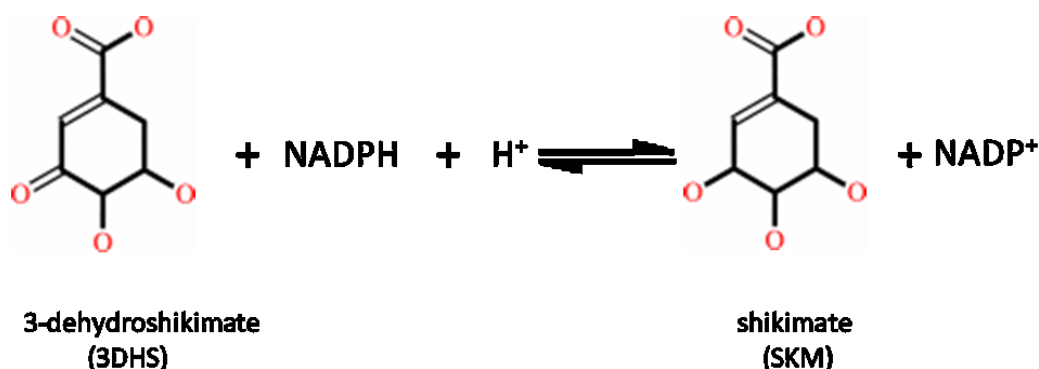


Figure 1. Reaction catalyzed by shikimate dehydrogenase (SDH).

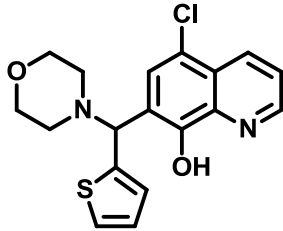
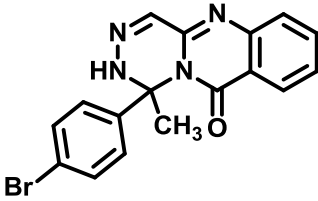
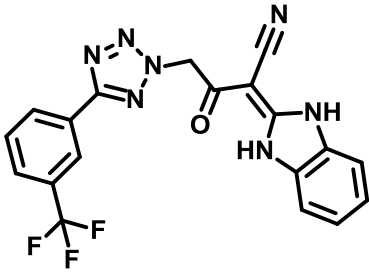
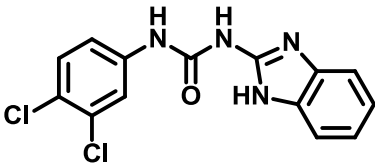
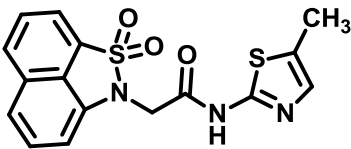
SDH exists in many bacteria as a single functional polypeptide, and in organisms like fungi and yeast, the enzyme is part of a multidomain pentafunctional enzyme catalyzing steps two to six of the shikimate pathway (9, 10). In plants, SDH is fused with 3-Dehydroquinate dehydratase, the third enzyme of shikimate pathway (11, 12). The homologs of SDH family display distinct biochemical functions, share low sequence identity, yet are structurally conserved. Within the five distinct classes, AroE is an archetypal SDH class found in most microbial organisms, using 3DHS / SKM as substrate and NADPH / NADP⁺ as cofactor (13, 14). YdiB class is a bifunctional reversible quinate/shikimate dehydrogenase with dual specificity for substrate (quinat and shikimate) and cofactor (NAD⁺ and NADP⁺) (15), occurs less widely in microbial organisms and is primarily implicated in the catabolic quinate utilization as a sole carbon source for growth (16, 17), in a NAD⁺ dependent manner. The physiological roles of three other classes, shikimate dehydrogenase-like (SdhL), AroE-like1 (Ael1) and RifI2 are unclear (18-20). Although, some microorganisms have paralogs of SDH encoding genes, *Mtb* genome analysis revealed a single gene *aroE* (Rv2552c), encoding SDH belonging to AroE class (3). The kinetic isotope and pH-rate profile studies of MtSDH propose that the hydride transfer and protonation of C3 group of 3DHS proceed in a concerted manner and that an amino acid with an apparent pK_a of 8.9 is involved in the catalytic activity (21). The *E. coli* SDH is known to stereo-specifically transfer C4-*proR* hydride of NADPH (22), which is consistent with the evidence from crystal structure of binary complex with the cofactor (15). However, in case of MtSDH, it is reported that

the C4-*proS* hydride of NADPH is stereo-specifically transferred in the oxy-reduction reaction on 3DHS (21). There is a well established correlation between the mode of NADPH binding and stereo-specific transfer by oxidoreductases and the molecular basis of this difference in MtSDH is unclear due to lack of three-dimensional structural analysis.

To date, crystal structures of SDH from 14 different species representing all five distinct classes have been determined and deposited in Protein Data Bank (PDB) (23). Structural analysis of AroE class of SDH describing the apo-enzyme, binary complex with substrate from *Staphylococcus epidermidis* SDH (SeSDH; PDB ID: 3DOO) (24) or cofactor from *E. coli* SDH (EcSDH; PDB ID: 1NYT) (15), inactive ternary complex from *Aquifex aeolicus* SDH (AaSDH; PDB ID: 2HK9_A) (25) and *Thermus thermophilus* SDH (TtSDH; PDB ID: 2EV9) (26) and an active ternary complex from AaSDH (PDBID: 2HK9_D) reveal conformational flexibility that manifest in open and closed forms of the enzyme. This conformational switch is linked to the activity of the enzyme, where the closed form is believed to be catalytically active form.

In this thesis, the crystal structures of MtSDH apo-enzyme and binary complex with SKM are reported. Additionally, selected inhibitors of MtSDH (Table 1) identified previously from a high-throughput enzyme assay screen are evaluated and characterized. The study provides a structural framework for efforts in rational design of inhibitors against MtSDH.

Table 1. Selected inhibitors of MtSDH.

Compound	ID	Structure	Name
2	EN:T0509-3962		5-chloro-7-(morpholino(thiophen-2-yl)methyl)quinolin-8-ol
5	EN:T0512-3612		1-(4-bromophenyl)-1-methyl-1H-[1,2,4]triazino[5,4-b]quinazolin-10(2H)-one
6	EN:T0514-6228		2-(1H-benzo[d]imidazol-2(3H)-ylidene)-3-oxo-4-(5-(3-(trifluoromethyl)phenyl)-2H-tetrazol-2-yl)butanenitrile
8	EN:T5232146		1-(1H-benzo[d]imidazol-2-yl)-3-(3,4-dichlorophenyl)urea
11	EN:T5690368		2-(1,1-dioxido-2H-naphtho[1,8-cd]isothiazol-2-yl)-N-(5-methylthiazol-2-yl)acetamide

2. EXPERIMENTAL PROCEDURES

2.1 Cloning, protein over-expression and purification

MtSDH encoding gene *AroE* (Rv2552c) was amplified by polymerase chain reaction (PCR) from the genomic DNA of *Mtb* H37Rv. The purified PCR product was digested and ligated with pET-30b expression vector (Novagen) at *NdeI* and *XhoI* restriction sites. The stop codon of the gene was excluded on the anti-sense primer to incorporate the vector encoded His-tag, resulting in a C-terminal His-tagged MtSDH. The following primers were used:

Sense primer

5'-ATACTTCATATGAGCGAAGGTCCCAAAAAAGCCGG-3' and

Anti-sense primer

5'- ATACTTCTCGAGGTCCAACGCGGCCAGCG-3'

The sequence of the coding region in MtSDH-pET30b expression construct was confirmed by DNA sequencing.

The MtSDH-pET30b expression construct was transformed into *E. coli* BL21 (DE3) over-expression strain (Novagen). The cell culture was grown at 18 °C in Terrific Broth media containing kanamycin 50 µg/mL (for selection) until the mid-log phase ($OD_{600} = 0.6-0.8$) and immediately incubated in ice cold water for 30-45 minutes. Over-expression of MtSDH was induced by addition of 1 mM isopropyl-β-D-1-thio-galactopyranoside (IPTG) to ice cold cell culture and grown at 18 °C overnight. The cells were harvested and resuspended in 50 mM Tris-HCl pH 7.5, 300 mM NaCl and 2

mM β -mercaptoethanol (buffer A) containing 20 μ g/mL DNase I, 2mM MgCl_2 and 1mM PMSF. The cells were lysed in M-110P Microfluidizer[®] processor at an operating pressure of 18,000 psi. The lysate was centrifuged at $30,000 \times g$ for 45 min at 4 °C and the clarified extract was filtered with 0.2 μ m syringe filter and loaded on HisTrap FF column (GE Healthcare Life Sciences), pre-equilibrated with Buffer A containing 20 mM imidazole (buffer B). After loading the lysate, the column was washed with 5 column volumes of buffer B, followed by 10 column volumes of buffer A containing 40 mM imidazole (buffer C). The protein was eluted with a gradient of 40-500 mM imidazole in buffer A. The fractions containing MtSDH were pooled and concentrated using Spin-X[®] UF (Corning[®]) concentrator. This concentrated protein was loaded on HiLoad 26/60 Superdex 200 prep grade (GE Healthcare Life Sciences) gel filtration column, pre-equilibrated with 10 mM Tris-HCl pH 7.5, 300 mM NaCl and 1 mM DTT (buffer D). The eluted protein was pooled and concentrated to 10 mg/mL for crystallization. Based on 4-12 % gradient SDS-PAGE gel (Bio-Rad), MtSDH was more than 95 % homogeneous. All protein purification and concentrating procedures were performed in 4 °C.

2.2 Crystallization, data collection and processing

Crystallization was performed by vapor diffusion method in sitting drop plates at 18 °C. Crystals were obtained for MtSDH (10 mg/mL) in presence of 500 μ M SKM in the condition containing 0.08 M sodium citrate pH 6.2, 1.54 M $(\text{NH}_4)_2\text{SO}_4$, 2.7 % 1,6-hexanediol and 0.1 M guanidine HCl. Crystals grew to maximum size in 15-20 days in

drops mixed with 0.4 μL protein mixture (MtSDH + SKM) and 0.4 μL of crystallization condition. Based on this crystallization condition, optimization was performed to obtain crystals for apo-MtSDH. The apo-MtSDH (10 mg/mL) crystallized in 0.1 M sodium citrate pH 6.2, 1.65 M $(\text{NH}_4)_2\text{SO}_4$, 2.7 % 1,6-hexanediol and 0.1 M guanidine HCl by vapor diffusion technique, mixing 0.4 μL protein with 0.4 μL of crystallization buffer in sitting drop plates at 18 °C and grew to maximum size in 15-20 days. Prior to data collection, the crystals were transferred to a cryoprotectant composed of 15 % glycerol in mother liquor for 15-20 seconds and immediately flash frozen in liquid nitrogen. Bromide-derivative crystals were prepared by soaking MtSDH-SKM co-crystal in cryoprotectant solution containing 1 M NaBr for 10 minutes. The crystals for MtSDH-shikimate complex were obtained by soaking MtSDH-SKM co-crystal in mother liquor containing 5 mM SKM for 30 minutes and transferred to cryoprotectant solution before flash freezing in liquid nitrogen.

Data sets were collected on beamlines 23-ID of General Medical Sciences and Cancer Institutes Structural Biology Facility and 19-ID of Structural Biology Center, Advanced Photon Source (APS), Argonne National Laboratory (ANL). For the bromide-derivative crystal, 720 frames were collected in 0.5° oscillation steps with 1sec exposure per frame at a wavelength of 0.92 Å, which is close to the absorption edge of bromine. A total of 120 and 240 frames were collected in 1° oscillation steps with 1 sec exposure per frame at a wavelength of 0.98 Å for the data sets of apo-MtSDH and MtSDH-shikimate complex crystals, respectively. Diffraction data was indexed, integrated and scaled using

HKL-2000 program package (27). Relevant statistics of data collection and processing are summarized in Table 2.

2.3 Structure solution and model refinement

Phase determination by single-wavelength anomalous diffraction (SAD) method was performed for bromide derivatized MtSDH – SKM cocrystal using *AutoSol* in PHENIX (28) software suite. The apo-MtSDH and MtSDH – SKM complex structure in $P 2_1 2_1 2$ space group was determined by molecular replacement method using *AutoMR* in PHENIX and with one MtSDH molecule as a starting model. Manual model building of missing residues and side chains from the initial model was carried out using *Coot* (29); and *phenix.refine* in PHENIX was used for refinement. The quality of all structural models were assessed with PROCHECK (30) and *MolProbity* (31). Figures and superpositions of structural models were generated using Chimera (32). The refinement statistics are summarized in Table 2.

Table 2. Summary of diffraction data and refinement statistics.

	Apo-MtSDH	Shikimate-MtSDH	Bromide-MtSDH
Data Collection			
Space group	P 2 ₁ 2 ₁ 2	P 2 ₁ 2 ₁ 2	P 2 ₁ 2 ₁ 2 ₁
Cell dimensions			
a, b, c (Å)	128.57, 132.70, 38.61	129.70, 132.31, 38.46	43.47, 75.55, 129.71
α , β , γ (°)	90, 90, 90	90, 90, 90	90, 90, 90
Wavelength (Å)	0.979	0.979	0.920
Resolution (Å)	50.0-1.95 (1.98-1.95)	50.0-2.03 (2.08-2.03)	50.0-1.70 (1.73-1.70)
Completeness (%)	99.30 (98.68)	98.42 (89.36)	99.47 (95.13)
Redundancy	4.4 (4.2)	9.0 (8.9)	7.3 (4.4)
I / σ	24.92 (8.81)	20.12 (2.62)	25.63 (4.38)
R _{sym}	0.057 (0.175)	0.066 (0.733)	0.088 (0.608)
Refinement			
Resolution (Å)	46.17-1.95	46.31-2.03	49.23-1.70
No. of reflections	49154	42809	47232
R _{work} / R _{free}	0.186 / 0.228	0.202 / 0.248	0.184 / 0.228
No. of Atoms			
Protein	5614	5596	3743
Ligand / ion	25	73	34
Water	346	102	495
B-factors (Å ²)			
Protein	22.7	48.1	16.6
Ligand / ion	27.6	44.4	28.0
Water	27.5	39.8	33.2
Rmsd			
Bond length (Å)	0.007	0.008	0.006
Bond angles (°)	1.12	1.14	1.10
Ramachandran plot			
Most favored (%)	96.0	95.0	95.1
Allowed (%)	4.0	5.0	4.9
Disallowed (%)	0	0	0

Values in parentheses are for highest resolution shell.

2.4 Differential scanning fluorimetry

Thermal profile of MtSDH was investigated in presence of substrates and inhibitors. In a 96-well thin wall PCR plate, the protein was diluted to a final assay concentration of 10 μM in 100 mM potassium phosphate buffer pH 7.4, 5 \times SYPRO[®] orange dye (Life Technologies) and 2.5% (v/v) DMSO. The final concentration of 3DHS and NADPH was 500 μM and stock solutions of compounds prepared in DMSO were diluted to 300 μM in the final assay volume of 20 μL . All measurements were taken in duplicate. After adding all the components, the PCR plate was centrifuged at 1500 rpm for 2 minutes and sealed with an optical quality adhesive film. Thermal denaturation was recorded using Mx3005P qPCR system (Agilent Technologies), with excitation and emission wavelengths of 492 nm and 610 nm, respectively, for SYPRO orange, applying a temperature gradient of 1 $^{\circ}\text{C}/\text{min}$ from 25 $^{\circ}\text{C}$ to 75 $^{\circ}\text{C}$. The midpoint temperature of protein thermal melting, T_m , was determined by fitting the base-line corrected raw fluorescence (dR) data to the Boltzmann sigmoid equation using GraphPad Prism 6 (GraphPad Software, Inc.). Fitting of data was judged from the goodness of fit ($R^2 > 0.98$).

2.5 MtSDH enzymatic assays

The MtSDH enzyme activity was assayed in 100 mM potassium phosphate buffer pH 7.4 containing final concentration of 0.5% (v/v) DMSO, by monitoring the oxidation of NADPH at 340 nm ($\epsilon_{340} = 6220 \text{ M}^{-1} \text{ cm}^{-1}$) in the presence of 3DHS at 25 $^{\circ}\text{C}$

in a final assay volume of 1 mL, with disposable acrylic cuvettes. The kinetic data were collected on Cary 100 UV-Vis spectrophotometer (Agilent Technologies) in triplicates. The initial velocities of enzyme activity were measured by titrating substrate (3DHS) or cofactor (NADPH), in presence of saturating concentration of the other. The reaction was initiated by addition of NADPH.

To investigate the dose-dependent inhibition effect, 8 nM of enzyme was incubated with compounds at concentrations of 0, 0.5, 1, 2, 4, 8, 16, 32, and 64 μM for 10 minutes before starting the reaction in presence of 40 μM 3DHS ($2\times$ times its K_m) and 150 μM NADPH ($15\times$ times its K_m). The IC_{50} values were derived by fitting the initial velocity data to a sigmoid dose-response equation in SigmaPlot™ 12.5 package (Systat Software, Inc.).

To investigate the mode of inhibition, substrate and cofactor were titrated in presence of saturating concentration of the other, at varied compound concentrations. 3DHS was titrated in the concentrations of 15, 30, 60, 120, and 240 μM while NADPH was maintained at 200 μM . NADPH was titrated in the concentrations of 5, 10, 20, 40, and 80 μM while 3DHS was maintained at 200 μM . Initial velocities were measured with compounds **2**, **6** and **8** varied at concentrations of 0, 3, 4.5, and 6 μM , whereas with compounds **5** and **11** concentrations were varied at 0, 2, 3.5 and 5 μM . The kinetic parameters, Michaelis constants, K_m , and maximal rates, V_{max} , were derived by fitting data to Michaelis-Menten equation and was judged from the goodness of fit ($R^2 > 0.98$). SigmaPlot™ 12.5 (Systat Software, Inc.) was used for all kinetic data analysis and plots.

3. RESULTS AND DISCUSSION

3.1 Structure determination of MtSDH

Three dimensional co-crystals of MtSDH-SKM were optimized and bromide derivatives were produced by soaking them for 10 minutes in cryoprotectant solution containing 1 M NaBr. Bromide-SAD data was collected to 1.7 Å resolution and the crystal belonged to primitive orthorhombic space group $P 2_1 2_1 2_1$ containing 2 molecules in an asymmetric unit with solvent content of ~28%. The anomalous signal was significant to ~2.2 Å. Substructure solution using *PHENIX* (28) *AutoSol* initially located 67 bromide sites with a figure of merit (FOM) of 0.39. A partial preliminary model was subjected to iterative model building and refinement with *AutoBuild*, which automatically built 470 residues and 334 side chains with R_{work} and R_{free} values of 29.3 % and 32.6 %, respectively. This model was subsequently refined with few rounds of noncrystallographic symmetry restraints using *phenix.refine*. Missing residue side chains were built manually into $2F_o - F_c$ and $F_o - F_c$ electron-density maps and further refined. The final R_{work} and R_{free} was 18.4 % and 22.8 %, respectively.

The density of shikimate in the bromide derivatized cocrystal of MtSDH-SKM was partial. Therefore, the cocrystal of MtSDH-SKM was soaked additionally for 30 minutes in 5mM SKM, prepared in mother liquor and flash frozen with cryoprotectant before data collection. Data was collected to 2.03 Å resolution and the MtSDH-shikimate binary complex crystal belonged to primitive orthorhombic $P 2_1 2_1 2$ space group containing 3 molecules in an asymmetric unit and a larger unit cell, different from

bromide derivatized crystal. An initial model of MtSDH-shikimate binary complex was obtained by molecular replacement method using *AutoMR* in *PHENIX* due to the difference in unit cell and space group. This model was subjected to iterative model building and refinement using *AutoBuild*, followed by rigid-body refinement and subsequent rounds of noncrystallographic symmetry restraints refinement using *phenix.refine*. Unambiguous density of shikimate was observed in difference Fourier maps in all 3 molecules of the asymmetric unit. The R_{work} and R_{free} of the final model was 20.2 % and 24.8 %, respectively.

The optimized apo-MtSDH crystals diffracted to a resolution of 1.95 Å and belonged to primitive orthorhombic $P 2_1 2_1 2$ space group containing 3 molecules in an asymmetric unit and unit cell dimensions similar to MtSDH-shikimate binary complex crystal. The model of apo-MtSDH was obtained by refining data against the structure of MtSDH-shikimate (excluding ligand and heteroatoms) using *phenix.refine*. The final R_{work} and R_{free} of the apo-MtSDH was 18.6 % and 22.8 %, respectively. All the three structures' stereochemistry was analyzed by PROCHECK and no outliers were seen in the Ramachandran plot.

3.2 Overall structure of apo-MtSDH and binary complex with shikimate

The structures were obtained in two crystal forms. The bromide soaked co-crystal of MtSDH-shikimate binary complex was obtained in crystal form I (space group $P2_1 2_1 2_1$) with two crystallographically independent molecules per asymmetric unit, solved at 1.7 Å resolution. The apo-enzyme and co-crystal MtSDH-shikimate further

soaked with shikimate were obtained in crystal form II (space group $P 2_1 2_1 2$) with three crystallographically independent molecules per asymmetric unit, solved at 1.95 Å and 2.03 Å resolution, respectively.

The apo-MtSDH structure contains 788 amino acids (residues 5 – 268 for subunit A, 5 – 265 for subunit B, and 5 – 267 for subunit C), 5 sulfate ions and 346 water molecules. The binary structure of MtSDH-shikimate in crystal form I contains 525 amino acids (residues 5 – 267 for subunits A and B, the loop containing residues 173 – 177 is disordered in subunit B), one shikimate molecule in subunit A, 7 bromide ions, 3 sulfate ions and 495 water molecules. Whereas the crystal form II contains 784 amino acids (residues 5 – 267 for subunits A, B and C, residues 117, 175 – 180 from subunit B and residue 118 from subunit C were not built due to lack of backbone density), three shikimate molecules, 5 sulfate ions and 102 water molecules. The shikimate molecules adopt half-chair conformation. In all crystal forms, strong density was found near Arg149, in which sulfate was fit in a satisfactory manner.

The overall structure of MtSDH is modular with two structural domains containing α/β architecture (Figure 2), similar to other SDH structures. The N-terminal substrate binding domain is formed by two discontinuous segments composed of residues 5 – 108 and 241 – 267, containing six-stranded β -sheet in the order $\beta 2$, $\beta 1$, $\beta 3$, $\beta 5$, $\beta 6$ and $\beta 4$ with $\beta 5$ strand being anti-parallel to other strands. Helices $\alpha 1$, $\alpha 13$ and $\alpha 14$ flank these strands on one side and on the other side are helices $\alpha 2$, $\alpha 3$ and $\alpha 4$. The C-terminal cofactor binding domain composed of residues 109 – 240 adopts a Rossmann fold containing six-stranded parallel β -sheet in the order $\beta 9$, $\beta 8$, $\beta 7$, $\beta 10$, $\beta 11$ and $\beta 12$,

flanked by helices $\alpha 6$ and $\alpha 7$ on the inner side and $\alpha 8$, $\alpha 9$, $\eta 10$ (3_{10} helix), $\alpha 11$ and $\alpha 12$ on the outer side. In other SDH structures, $\beta 10$ and $\beta 11$ strand are connected by a long loop. However, in MtSDH this loop is replaced by a series of $\alpha 9$, $\eta 10$ and $\alpha 11$ helices. Between the two domains are interconnecting helices $\alpha 5$ and $\alpha 13$ forming a groove in which substrate and cofactor bind for catalysis.

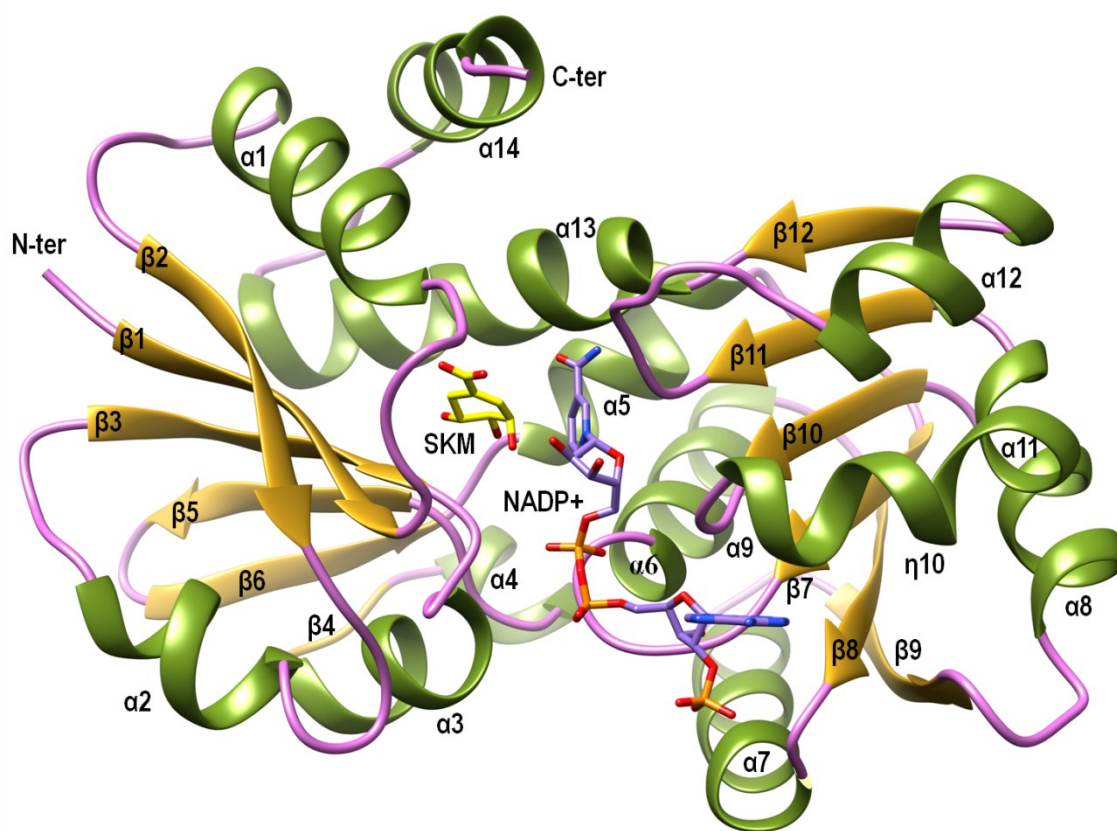


Figure 2. Overall structure of MtSDH. The structure is shown as cartoon. Secondary structural elements are colored as follows: helices in green, sheets in gold, loops in orchid. The ligands are colored by heteroatoms with carbons for SKM in yellow and in purple for NADP^+ (modeled by superposition of *Aquifex aeolicus* SDH structure on MtSDH).

3.3 Conformational flexibility of MtSDH

The conformational flexibility of SDH is observed and reported for different structures. The flexibility results in domain movements and manifests in various degrees of open and closed form of SDH, which is related to the activity of the enzyme. The crystal structures of both apo-MtSDH and MtSDH-shikimate binary complex are in a closed conformation when compared to other known open conformation of SDH homologs. The co-crystal structure in crystal form I is in a more closed conformation than the structures in crystal form II and this conformational difference in MtSDH is attributed to the hinge residues ¹⁰⁵Asp-Ile-Asp¹⁰⁷ and ²³⁸Gln-Met-Leu-Leu²⁴¹ within the α -helices ($\alpha 5$ and $\alpha 13$) linking the two domains of the protein (Figure 3). The domain movements correspond to $\sim 11^\circ$ rotation around an axis passing through C α of Asp105 and Leu241. The backbone root mean square deviation (Rmsd) between the two conformations is 0.48 Å and 0.36 Å for N-terminal substrate binding domain and C-terminal cofactor binding domain, respectively.

Determined bond distances between some key residues in the substrate binding and cofactor binding sites are characteristic of the open and closed form of SDH (24). Among these are the distance between C α of catalytic lysine and the invariant central glycine in Gly-Ala-Gly-Gly-Ala motif and the distance between C α of conserved tyrosine and two serines in the substrate binding pocket. In MtSDH, the C α of catalytic Lys69 and invariant Gly126 are at a distance of 8.9 Å, and the distance between C α of conserved Tyr215 – Ser18 and Tyr215 – Ser20 are 9.1 Å and 11.5 Å, respectively (Figure 3). These bond distances are very similar to those observed in the closed active

ternary complex of AaSDH (25), in contrast to open conformation of SeSDH (24).

Taken together, the MtSDH structure represents a closed conformation, equivalent to catalytically active form.

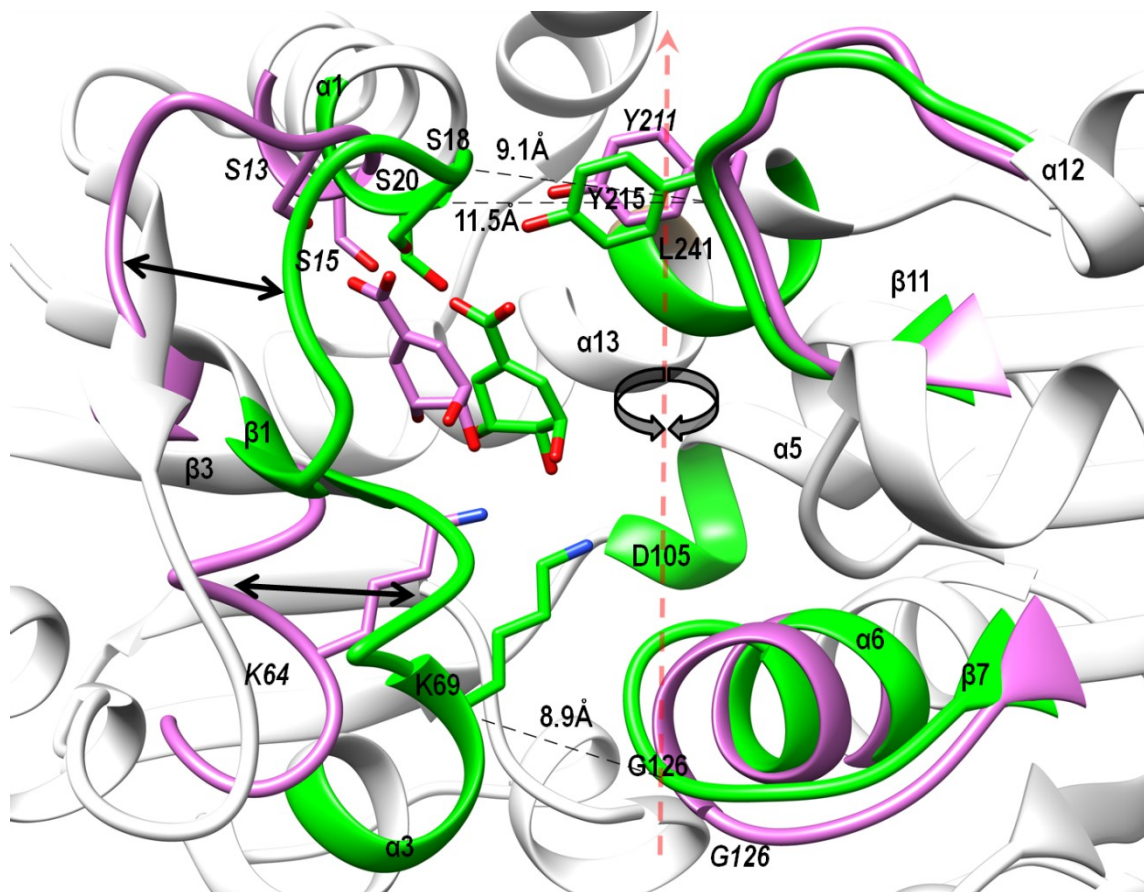


Figure 3. Structural elements of MtSDH closed conformation. Superposition of MtSDH and SeSDH structures. Partial MtSDH is shown in white cartoon. The carbons corresponding to residues that show prominent movement between the MtSDH and SeSDH are highlighted in green and orchid colors, respectively. The SKM is colored according to the enzyme it is bound to. The distance between key residues that define the open or closed conformation, K69-G126, Y215-S18 and Y215-S20 in MtSDH are shown. The axis passing through D105 and L241 resulting in domain movement is shown in red broken arrow. The extent of shift in structural elements between MtSDH and SeSDH are indicated in black two-sided arrows.

3.4 Analysis of the substrate-binding domain

The substrate binding domain is structurally well conserved in SDH enzymes. The SKM binding site is in a pocket formed between the N-terminal substrate binding domain and the C-terminal cofactor binding domain. In the binary structure of MtSDH, the density for SKM is unambiguous and adopts a half-chair conformation with the C3-O bond positioned orthogonal to its ring system (Figure 4A). SKM is situated near β 1, β 3, β 5 strands, α 3 helix and interconnecting loops at the bottom and surrounded by α 1, α 13 and α 14 helices on the top. The carboxylate group and three (C3, C4 and C5) hydroxyl groups of SKM interact with several residues in the pocket (Figure 4B). The carboxylate group makes hydrogen bonds with highly conserved side chains of Ser18-OG (2.4 Å) and Ser20-OG (2.7 Å). Substitution of the first conserved serine has been shown to have significant effect on the affinity of substrate and substitution of the second conserved serine affected both affinity and catalysis in SDH from *Arabidopsis thaliana* (33). Pro14 and Pro21 are also highly conserved and may play a role in optimal positioning of the conserved serines to form stable interaction with the carboxylate of SKM. Tyr215 is located in the cofactor binding domain, however its side chain extends into the SKM binding pocket allowing Tyr-OH (2.5 Å) to hydrogen bond with the carboxylate group of SKM. Although, Tyr215 is not catalytically involved, substitution has been shown to affect catalysis, suggesting its role in stabilizing the catalytic intermediate, rather than initial binding (24, 33). The C5-hydroxyl forms hydrogen bond with the side chains of Asn90-ND2 (3.5 Å) and Gln243-OE1 (3.1 Å). In some SDH homologs, hydrogen bonding is formed with an additional conserved Asn located near

the C5-hydroxyl, which is replaced with Ser63 in MtSDH and is too distant to form hydrogen bond. The C4-hydroxyl forms hydrogen bonds with the side chains of conserved Lys69-NZ (3.4 Å), Asn90-ND2 (2.9 Å) and Asp105-OD1 (2.6 Å). The C3-hydroxyl is hydrogen bonded to Thr65-OG1 (2.9 Å) and conserved Lys69-NZ (2.9 Å). The presence of Pro67 probably assists in positioning the side chain of Lys69. Invariant residues corresponding to Lys69 and Asp105 of MtSDH are known to be absolutely essential for catalysis in AroE class of SDH. Interestingly, mutation of equivalent Lys and Asp residues in SdhL of *H. influenzae* and AroE of *A. thaliana* reduced activity to undetectable level (18, 33), whereas mutagenesis of these residues in *E. coli* YdiB indicated their role in substrate binding (34).

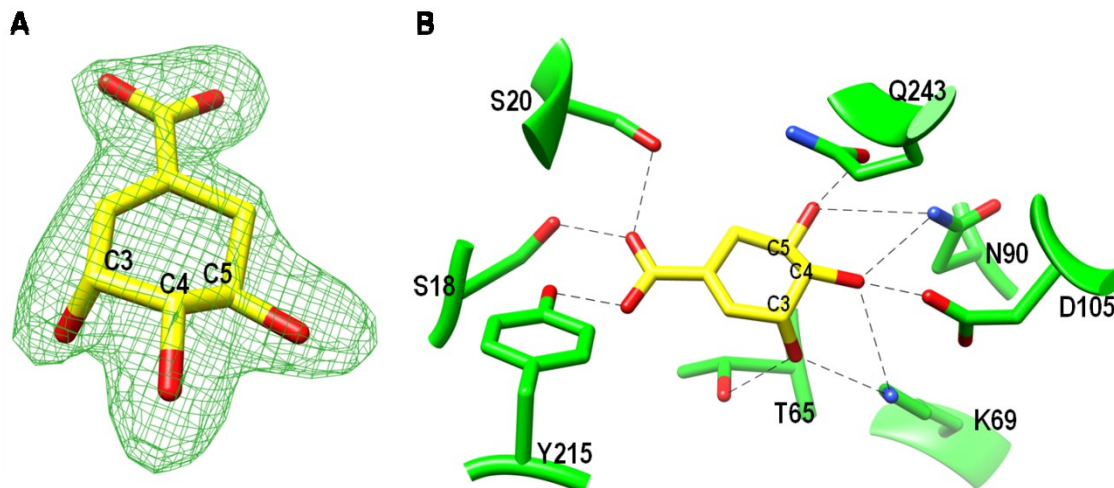


Figure 4. Shikimate and its interactions with MtSDH. (A) $F_o - F_c$ OMIT map of SKM contoured at 3σ level based on the final refined coordinates of MtSDH. (B) Specific interactions of the residue sidechains of MtSDH (carbons in green) and bound SKM (carbons in yellow) are shown in sticks and lines.

3.5 Analysis of the cofactor-binding domain

Attempts to obtain MtSDH structures of binary complex with cofactor NADP(H) or the ternary complex with substrate and cofactor have been unsuccessful. Comparison of MtSDH sequence with other structurally characterized bacterial AroE class of SDH enzymes show less than 25% sequence identity, however, they share strong structural similarity. Structure based sequence alignment of SDHs allow the identification of well conserved cofactor binding motifs. A glycine rich loop, a “basic patch” and the nicotinamide binding residues form the structurally conserved NADP(H) binding motifs and are present in MtSDH. Although, there are small differences in the sequence motif of glycine rich loop and the basic patch, NADP⁺ could be reliably modeled in the binding site by superimposing with SDH homologous structures containing the cofactor. The ternary structure of AaSDH bound with shikimate and NADP⁺ (PDB ID: 2HK9, Chain D) represents a catalytically competent closed conformation of the enzyme (25).

The NADP⁺ was modeled into the co-crystal structure of MtSDH bound with SKM by superimposing with the ternary structure of AaSDH. Based on this model and analysis of conserved residues in the region, the positioning of NADP⁺ in the MtSDH structure offers insight into relevant enzyme-cofactor interactions (Figure 5). The carbonyl O7 atom of nicotinamide ring should form hydrogen bond with main chain nitrogen of Leu240, while the N7 atom of nicotinamide ring makes hydrogen bonds with main chain oxygen of Ala213 and invariant Gly236. These interactions are key in determining the mode of NADP(H) binding. This specific interaction between the cofactor and enzyme retains the nicotinamide ring in *anti* conformation with respect to

the ribose. The nicotinic ribose maintains mostly non-polar interactions with residues in the loop region between strand $\beta 11$ and $\alpha 12$ helix.

The motif of the glycine rich loop is typically composed of Gly-Ala-Gly-Gly-Ala-Ala/Ser in most SDHs. However, the glycine rich loop of MtSDH, located between strand $\beta 7$ and $\alpha 6$ helix is made up of ¹²⁴Gly-Ser-Gly-Gly-Thr-Ala¹²⁹ residues. The main chain nitrogen of Ser125 should form hydrogen bonds with the 3'-hydroxyl of adenine ribose while the main chain nitrogen of Gly127 and Thr128 form hydrogen bonds with the diphosphate moiety. The adenine group lies in the pocket facing its A-side to the “basic patch” and the B-side to residues from loop between strand $\beta 10$ and $\alpha 9$ helix. The residues from the first turn in $\alpha 9$ helix are also involved in interactions. The consensus sequence of the “basic patch” motif is Asn-Arg-Thr-Xaa-Xaa-Arg/Lys and in MtSDH it is composed of residues ¹⁴⁸Ala-Arg-Asn-Ser-Asp-Lys¹⁵³, present within the preceding loop and part of $\alpha 7$ helix region. The residues interacting with the 2'-phosphate of adenine ribose are known to confer specificity for NADP(H) over NAD(H). In all the structurally characterized AroE class of SDH, adenosine 2'-phosphate interacts exclusively with the basic patch residues, primarily with side chains of invariant Arg (P2) along with Asn (P1) or/and Arg/Lys (P6). In some structures, additional bonding with side chain of Thr (P3) provides stability to phosphate binding. In our model, there is steric clash of adenine ring with the residues in the pocket on both sides. Therefore, these residues would have to move to accommodate the adenine ring in the pocket. In MtSDH, the $\alpha 9$, $\eta 10$ and $\alpha 11$ helices facing the B-side of adenine ring replace a long loop found in all the other SDH structures solved to date. It is possible that this region

may undergo structural change upon NADP(H) binding. Similarly, the residues in the basic patch may rearrange on the A-side of the adenine to accommodate the plausible cation – π interaction and hydrogen bonding interaction of Arg149 side chain with the adenine ring and adenosine 2'-phosphate, respectively. In fact, the electron density in this region is weak, suggesting the mobility of residues in absence of NADP(H).

In MtSDH structure, a sulfate ion was fit into electron density very close to Arg149 in a satisfactory manner, which potentially corresponds to positioning of adenosine 2'-phosphate. In the model Arg149 and Asn150 from the basic patch are indeed within hydrogen bonding distance for interactions with 2'-phosphate of adenine ribose. Additionally, the side chain of Ser125-OG atom in the glycine rich loop is within hydrogen bonding distance of adenosine 2'-phosphate. Together Arg149, Asn150 and Ser125 could recognize the terminal phosphate moiety and reveal a novel cofactor binding microenvironment in SDH family of enzymes.

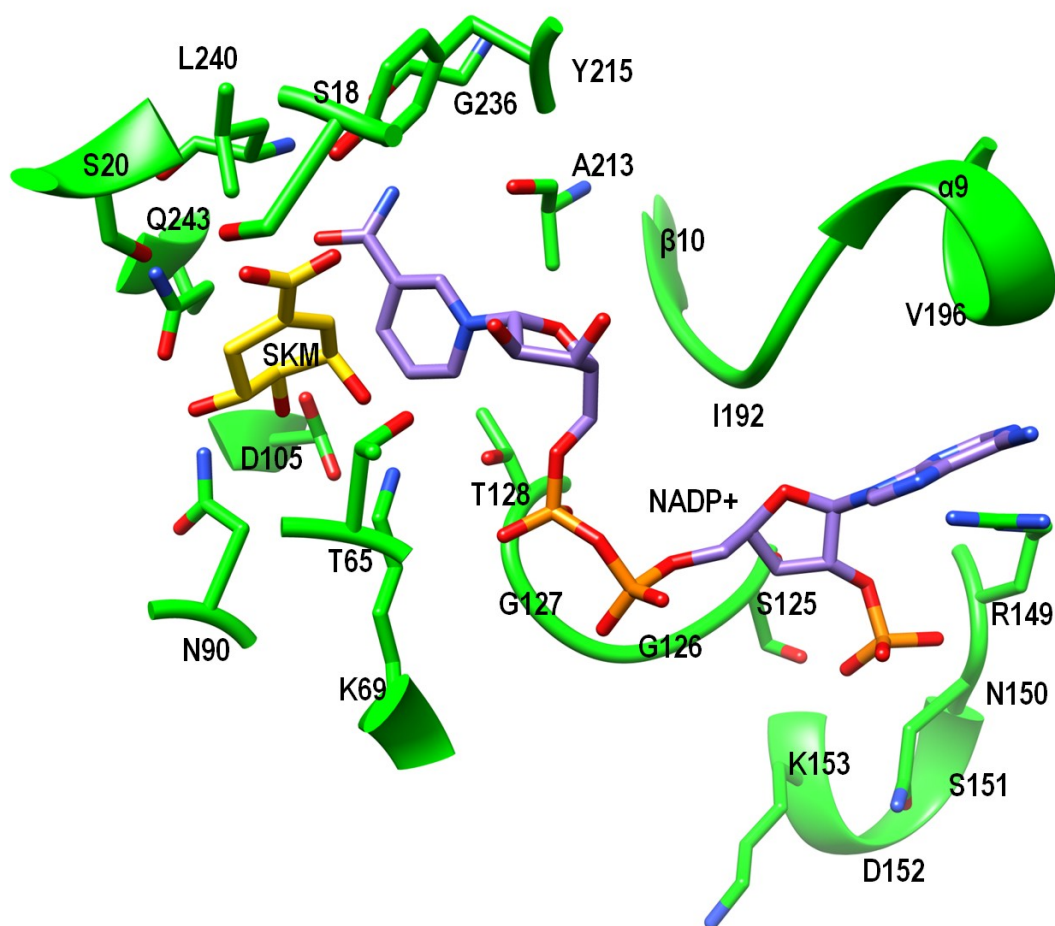


Figure 5. Interactions of MtSDH with shikimate and NADP⁺. The MtSDH residues, SKM and modeled NADP⁺ carbons are colored in green, yellow and purple, respectively. Only selective residue side chains interacting with SKM or NADP⁺ are shown for clarity.

3.6 Mode of substrate and cofactor-binding, recognition and catalysis

The binary complex crystal structure of MtSDH with shikimate in crystal form I represents a closed conformation. The NADP⁺ modeled into the binary complex of MtSDH – SKM by superimposition with the ternary structure of AaSDH bound with SKM and NADP⁺ allows for detailed understanding of the interactions and their

implication in enzyme catalysis. An earlier study reporting the kinetic and chemical mechanism of MtSDH proposed an ordered bi-bi mechanism with initial binding of 3-dehydroshikimate followed by NADPH, consequently transferring the C4-*proS* hydride from NADPH and proton from an amino acid residue with an apparent pK_a of 8.9 in a concerted manner (21). Subsequently, site-directed mutagenesis study showed that Lys69 is a critical residue for catalysis (35). A common proposition in the reaction catalyzed by SDH is the role of invariant lysine and aspartate forming catalytic dyad, functioning in a general acid-base mechanism during catalysis.

It is evident from the binary structure of MtSDH with SKM that these corresponding residues, Lys69 and Asp105 are in close proximity of the reactive C3-hydroxyl of SKM. In addition, based on the ternary model of MtSDH, C4 of the nicotinamide ring from cofactor is positioned within 3.5 Å distance to receive hydride from C3 of SKM. Based on MtSDH crystal structure and biochemical literature, it could be suggested that Lys69 side chain acts as an acid/base catalytic group donating a proton to 3DHS during the reduction reaction and removing a proton from SKM in the oxidation reaction, while Asp105 may play an important role in both substrate binding and catalysis by mediating proton transfer between Lys69 and a conserved water molecule found in many homologous SDH structures.

It is well established that the hydride transfer catalyzed by oxidoreductases is stereo-specific and correlated to the binding mode of cofactor. The key determinant of cofactor conformation is the interaction of the amide group of nicotinamide ring with the protein to orient it in *anti* or *syn* conformation, and accordingly transfer *pro-R* or *pro-S*

hydride, respectively. It has been shown that *E. coli* SDH transfers the C4-*proR* hydride (A-side) of NADP(H) (22), consistent with *anti* conformation of the cofactor in the crystal structures. Whereas, similar biochemical studies on MtSDH indicate the transfer of C4-*proS* hydride (B-side) from NADPH in the oxy-reduction reaction (21), suggesting that cofactor will bind to the enzyme in *syn* conformation. However, the evidence from binary MtSDH crystal structure with SKM and modeled NADP⁺ demonstrates that the cofactor would bind in *anti* conformation and consequently transfer C4-*proR* hydride (A-side). It could be hypothesized, that the cofactor may bind in different modes in oxidation and reduction states. Such observations have been made in crystal structures of UDP-glucose-4-epimerase and GDP-fucose synthetase enzymes from *E. coli*, but it was observed that the orientation of the nicotinamide ring with respect to ribose is dependent on the presence or absence of substrate (36-38). In MtSDH, the presence of substrate would confine the cofactor binding in *anti* mode to transfer C4-*proR* hydride (A-side), while the enzyme maintains a closed conformation during catalysis. In the event, the cofactor assumes *syn* conformation, there will be steric clash with the substrate. In order to avoid the clash and accommodate the cofactor in *syn* conformation the substrate would have to move; which will consequently require opening of the active site exposing it to the bulk solvent and the redox reaction is unlikely to occur under such conditions.

3.7 MtSDH thermal denaturation profiles with substrates and inhibitors

To test the binding of MtSDH inhibitors, identified previously from high-throughput screening, thermal shift or differential scanning fluorimetry (DSF) assay was performed. A list of selected inhibitors is shown in Table 1. Thermal profile of MtSDH denaturation was assessed by following the fluorescence change of environmentally sensitive SYPRO Orange dye (Figure 6). The apo MtSDH showed a monophasic transition with a melting point, T_m of 57.38 ± 0.03 °C. This condition allowed thermal profiling of MtSDH with substrates and inhibitors (Table 3). The T_m shift of protein in presence of substrates or compounds is indicative of binding interactions with the ligand. In most cases, the ligand binding stabilizes the protein thus making a positive shift in T_m . However, a ligand interaction could de-stabilize the protein, shifting the T_m negatively. The T_m shift of MtSDH in the presence of 3DHS and NADPH was 1.3 °C and 2.4 °C, respectively. While the T_m shift was 5.6 °C in presence of both 3DHS and NADPH, suggesting that substrate and cofactor binding provide more stability to MtSDH.

Thermal denaturation of MtSDH was done with the inhibitors. Compounds **2**, **6**, **8** and **11** showed significant T_m shift compared to controls (apo enzyme, in presence of 3DHS, NADPH and in presence of both 3DHS and NADPH). There was no significant T_m shift observed for compound **5** under the performed assay conditions. The T_m of MtSDH increased with compound **6** and **11** by 4.8 °C and 2 °C, respectively. Whereas the T_m of MtSDH decreased with compound **2** by 13.0 °C, indicating that these compounds have binding interactions with MtSDH. The T_m with compound **2** in presence of 3DHS or NADPH did not vary significantly compared to free enzyme.

However the presence of both substrate and cofactor was able to counter the destabilizing effect of the compound. Compound **6** showed more T_m shift of MtSDH, compared to T_m shift in the presence of substrate or cofactor, indicating it can bind better to free enzyme than the enzyme-substrate/cofactor complex. The T_m of MtSDH in the presence of compound **8** could not be determined because the melting point transition was not monophasic. The T_m shift with Compound **11** was similar for free enzyme and in the presence of 3DHS compared to presence of NADPH.

Table 3. Transition melting point, T_m of MtSDH. T_m determined from non-linear regression fit to Boltzmann sigmoidal equation.

	DMSO Control	Compound			
		2	5	6	11
AroE	57.38 °C ±0.03	44.34 °C ±0.1	57.50°C ±0.1	62.13 °C ±0.08	59.35 °C ±0.05
AroE + 3DHS	58.7 °C ±0.08	42.82 °C ±0.1	59.09 °C ±0.15	62.87 °C ±0.07	62.25 °C ±0.2
AroE + NADPH	59.76 °C ±0.08	44.18 °C ±0.1	59.07 °C ±0.07	63.16 °C ±0.07	61.68 °C ±0.07
AroE + 3DHS + NADPH	63.0 °C ±0.06	49.88 °C ±0.15	63.15 °C ±0.1	65.7 °C ±0.1	64.92 °C ±0.12

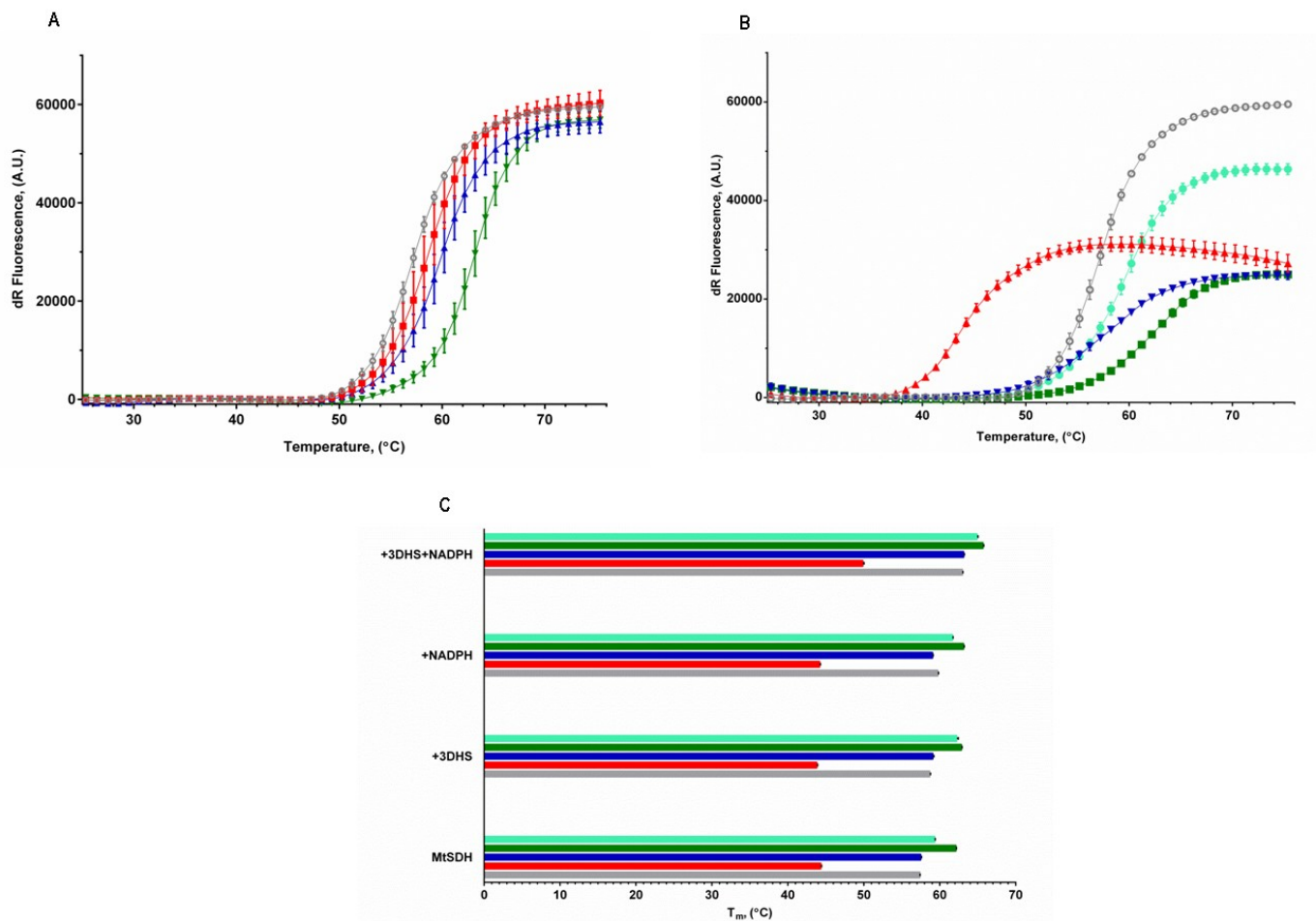


Figure 6. Thermal denaturation profile of MtSDH. (A) MtSDH (○), +3DHS (■), +NADPH (▲), +3DHS+NADPH (▼); (B) MtSDH (○), +Compound 2 (▲), +Compound 5 (▼), +Compound 6 (■), +Compound 11 (●); (C) Thermal stability dependence of MtSDH on substrates and inhibitors (Bar colors same as in B).

3.8 MtSDH initial velocity studies and evaluation of inhibitors

Catalytic properties of MtSDH were investigated in the direction of formation of SKM and NADP⁺. The apparent K_m for 3DHS and NADPH were determined to be $21.3 \pm 0.5 \mu\text{M}$ and $9.6 \pm 0.6 \mu\text{M}$, respectively, similar to previously reported values (39). MtSDH catalyzed the reduction of 3DHS at a maximal rate, V_{max} , of $64.1 \pm 0.4 \mu\text{mol min}^{-1} \text{mg}^{-1}$ with a catalytic constant, k_{cat} , of about 29 sec^{-1} and at catalytic efficiency, k_{cat}/K_m of $1.4 \times 10^6 \text{ M}^{-1} \text{ sec}^{-1}$. Whereas the oxidation of NADPH was catalyzed at a maximal rate, V_{max} , of $68.6 \pm 1.3 \mu\text{mol min}^{-1} \text{mg}^{-1}$ with a catalytic constant, k_{cat} , of about 31 sec^{-1} and at catalytic efficiency, k_{cat}/K_m of $3.3 \times 10^6 \text{ M}^{-1} \text{ sec}^{-1}$.

Dose-dependent inhibition of MtSDH inhibitors (Figure 7) was evaluated. All the five compounds inhibited MtSDH at low micromolar concentrations. The IC_{50} values for compounds **2**, **5**, **6**, **8** and **11** were $3.2 \pm 0.4 \mu\text{M}$, $3.0 \pm 0.2 \mu\text{M}$, $4.6 \pm 0.3 \mu\text{M}$, $3.9 \pm 0.4 \mu\text{M}$ and $2.8 \pm 0.1 \mu\text{M}$, respectively.

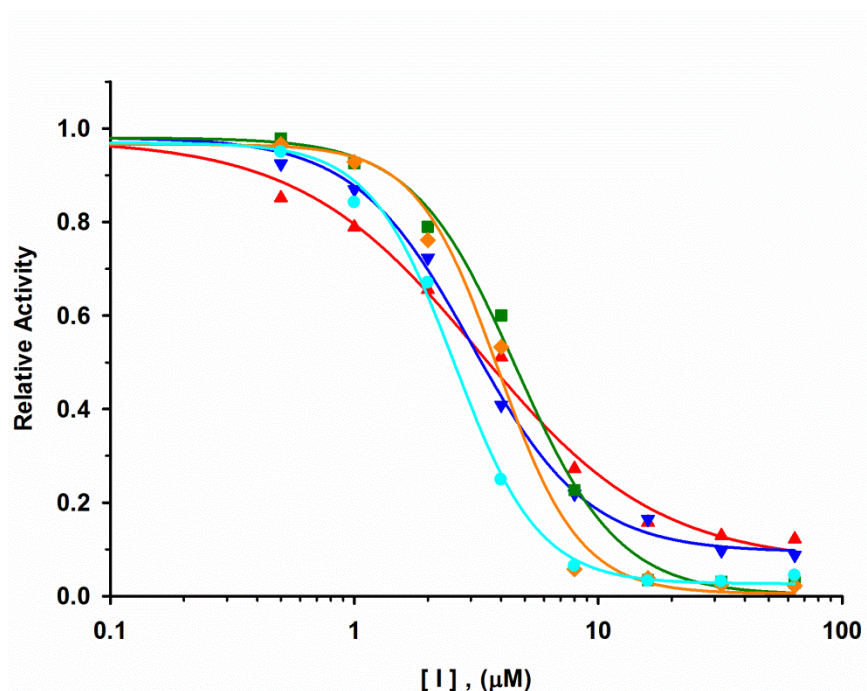


Figure 7. Dose-dependent inhibition of MtSDH. Compound **2** (▲), **5** (▼), **6** (■), **8** (◆), and **11** (●).

The mode of inhibition was explored by determining the dependence of MtSDH activity on 3DHS and NADPH concentrations, in the absence and presence of inhibitors (Tables 4 and 5). Titration with 3DHS, affected the V_{\max} of MtSDH by decreasing it by ~40% against compounds **2**, **5** and **8**, whereas with compounds **6** and **11**, it decreased by ~45% and 50%, respectively, at highest concentrations tested. Concurrently, the apparent K_m of 3DHS increased in presence of all the compounds. Consequently, the effect on catalytic efficiency, k_{cat}/K_m , of MtSDH was observed with all the compounds. Compounds **2** and **8** decreased the efficiency to $0.5 \times 10^6 \text{ M}^{-1} \text{ sec}^{-1}$, about 3-fold compared to control. Whereas compounds **5** and **11** decreased the efficiency to 0.6×10^6

$\text{M}^{-1} \text{sec}^{-1}$ and $0.4 \times 10^6 \text{ M}^{-1} \text{sec}^{-1}$, respectively. For the concentrations tested, compound **6** showed most effect, decreasing efficiency to $0.3 \times 10^6 \text{ M}^{-1} \text{sec}^{-1}$, more than 4-fold compared to control.

Similarly, when titrating with NADPH, the V_{max} of MtSDH decreased while there was a concomitant increase in the apparent K_{m} in presence of compounds, consequently also reducing the catalytic efficiency of MtSDH. For the concentrations tested, the catalytic efficiency, $k_{\text{cat}}/K_{\text{m}}$, was affected most in the presence of compounds **5** and **11**, reducing it to $0.7 \times 10^6 \text{ M}^{-1} \text{sec}^{-1}$, more than 5-fold compared to control. Whereas compounds **6** and **8** reduced the efficiency to $0.9 \times 10^6 \text{ M}^{-1} \text{sec}^{-1}$ and $1.0 \times 10^6 \text{ M}^{-1} \text{sec}^{-1}$, respectively. Compound **2** was least effective, reducing the efficiency of MtSDH to $1.1 \times 10^6 \text{ M}^{-1} \text{sec}^{-1}$. The effects on K_{m} and reaction's V_{max} suggest that the tested compounds act in non-competitive or mixed mode of inhibition with respect to both substrate and cofactor.

Table 4. MtSDH inhibition kinetics toward 3DHS titration.

Compound	Conc. (μM)	K_m (μM)	V_{\max} ($\mu\text{mol min}^{-1} \text{mg}^{-1}$)	k_{cat} (sec^{-1})	k_{cat} / K_m ($\times 10^6 \text{ M}^{-1} \text{sec}^{-1}$)
3DHS control		21.3 \pm 0.5	64.1 \pm 0.4	29.1 \pm 0.2	1.4
2	3.0	26.8 \pm 1.5	51.7 \pm 0.8	23.4 \pm 0.4	0.9
	4.5	32.4 \pm 2.3	44.7 \pm 1.0	20.3 \pm 0.5	0.6
	6.0	34.9 \pm 1.2	37.9 \pm 0.4	17.2 \pm 0.2	0.5
5	2.0	23.8 \pm 0.7	54.5 \pm 0.4	24.7 \pm 0.2	1.0
	3.5	30.7 \pm 2.0	47.2 \pm 0.9	21.4 \pm 0.4	0.7
	5.0	30.6 \pm 1.5	37.5 \pm 0.5	17.0 \pm 0.2	0.6
6	3.0	28.8 \pm 0.7	54.0 \pm 0.4	24.5 \pm 0.2	0.9
	4.5	29.7 \pm 0.4	47.5 \pm 0.2	21.5 \pm 0.1	0.7
	6.0	47.1 \pm 1.5	36.1 \pm 0.4	16.4 \pm 0.2	0.3
8	3.0	30.3 \pm 1.5	61.1 \pm 0.9	27.7 \pm 0.4	0.9
	4.5	33.2 \pm 1.8	46.5 \pm 0.8	21.1 \pm 0.4	0.6
	6.0	38.7 \pm 1.3	38.8 \pm 0.4	17.6 \pm 0.2	0.5
11	2.0	25.8 \pm 0.9	54.2 \pm 0.5	24.6 \pm 0.2	1.0
	3.5	29.8 \pm 2.7	44.0 \pm 0.9	20.0 \pm 0.4	0.7
	5.0	40.7 \pm 2.8	33.2 \pm 0.8	15.1 \pm 0.4	0.4

Table 5. MtSDH inhibition kinetics toward NADPH titration.

Compound	Conc. (μM)	K_m (μM)	V_{\max} ($\mu\text{mol min}^{-1} \text{mg}^{-1}$)	k_{cat} (sec^{-1})	k_{cat} / K_m ($\times 10^6 \text{ M}^{-1} \text{sec}^{-1}$)
NADPH control		9.6 \pm 0.6	68.6 \pm 1.3	31.1 \pm 0.6	3.3
2	3.0	14.0 \pm 2.2	67.0 \pm 3.6	30.4 \pm 1.6	2.2
	4.5	16.4 \pm 2.0	62.5 \pm 2.8	28.3 \pm 1.3	1.7
	6.0	18.7 \pm 2.0	43.5 \pm 1.7	19.7 \pm 0.8	1.1
5	2.0	14.4 \pm 2.3	60.2 \pm 3.3	27.3 \pm 1.5	1.9
	3.5	18.8 \pm 2.0	52.8 \pm 2.0	23.9 \pm 1.0	1.3
	5.0	25.4 \pm 4.5	36.8 \pm 2.6	16.7 \pm 1.2	0.7
6	3.0	14.5 \pm 1.5	60.2 \pm 2.0	27.3 \pm 0.9	1.9
	4.5	22.2 \pm 2.9	55.5 \pm 2.8	25.2 \pm 1.3	1.1
	6.0	25.4 \pm 1.7	52.8 \pm 1.5	23.9 \pm 0.6	0.9
8	3.0	8.4 \pm 0.9	61.6 \pm 1.8	27.9 \pm 0.8	3.3
	4.5	15.7 \pm 0.6	48.2 \pm 0.6	21.9 \pm 0.3	1.4
	6.0	16.4 \pm 2.4	36.8 \pm 1.9	16.7 \pm 0.9	1.0
11	2.0	11.5 \pm 0.4	48.0 \pm 0.6	21.8 \pm 0.3	1.9
	3.5	14.8 \pm 1.7	43.0 \pm 1.7	19.5 \pm 0.8	1.3
	5.0	15.5 \pm 1.5	24.6 \pm 0.8	11.2 \pm 0.4	0.7

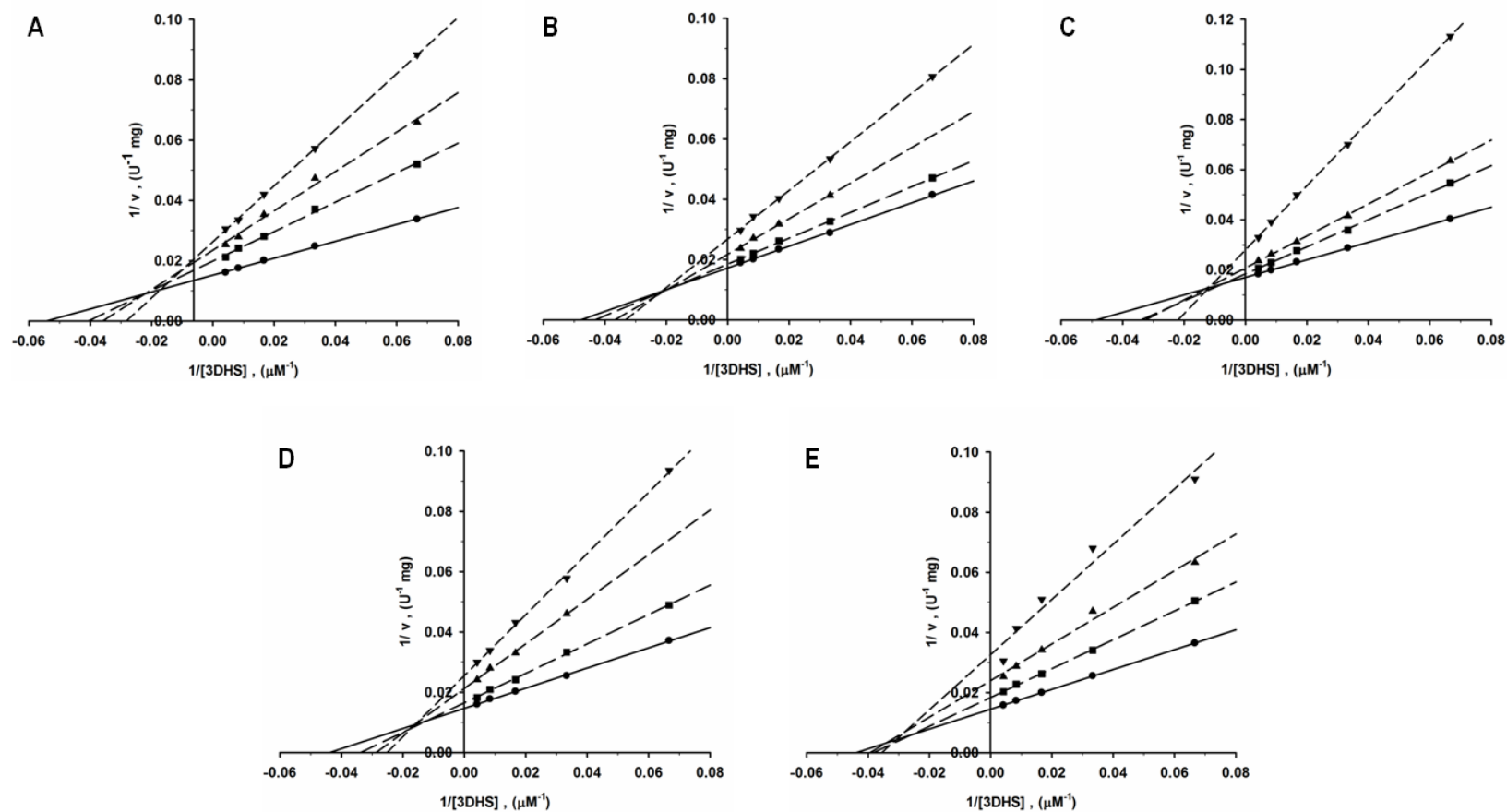


Figure 8. Inhibition of MtSDH toward 3DHS with increasing concentration of compounds. (A) Compound **2** [0 μM (●), 3 μM (■), 4.5 μM (▲), 6 μM (▼)]; (B) Compound **5** [0 μM (●), 2 μM (■), 3.5 μM (▲), 5 μM (▼)]; (C) Compound **6** [0 μM (●), 3 μM (■), 4.5 μM (▲), 6 μM (▼)]; (D) Compound **8** [0 μM (●), 3 μM (■), 4.5 μM (▲), 6 μM (▼)]; (E) Compound **11** [0 μM (●), 2 μM (■), 3.5 μM (▲), 5 μM (▼)].

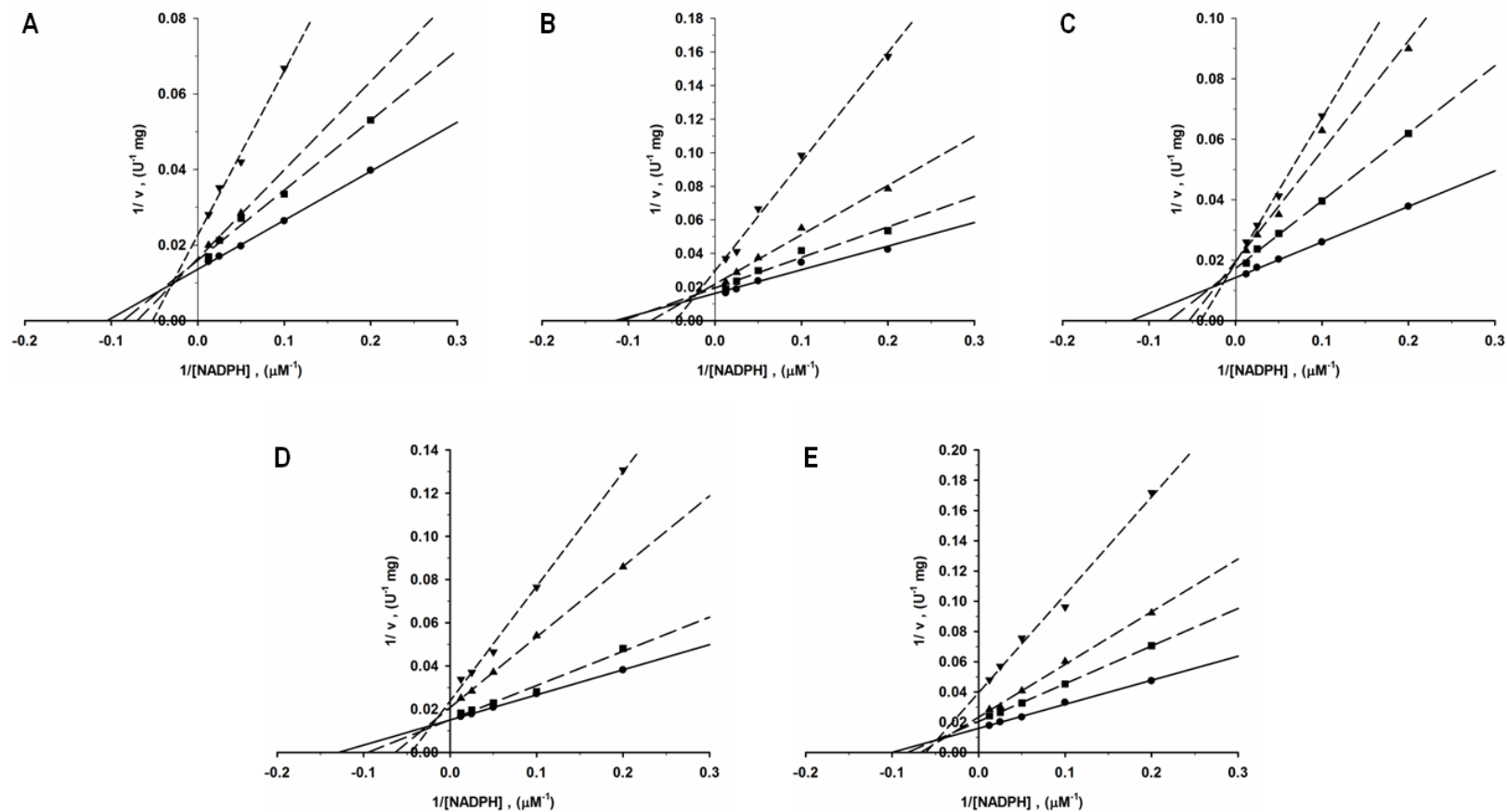


Figure 9. Inhibition of MtSDH toward NADPH with increasing concentration of compounds. (A) Compound 2 [0 μM (\bullet), 3 μM (\blacksquare), 4.5 μM (\blacktriangle), 6 μM (\blacktriangledown); (B) Compound 5 [0 μM (\bullet), 2 μM (\blacksquare), 3.5 μM (\blacktriangle), 5 μM (\blacktriangledown); (C) Compound 6 [0 μM (\bullet), 3 μM (\blacksquare), 4.5 μM (\blacktriangle), 6 μM (\blacktriangledown); (D) Compound 8 [0 μM (\bullet), 3 μM (\blacksquare), 4.5 μM (\blacktriangle), 6 μM (\blacktriangledown); (E) Compound 11 [0 μM (\bullet), 2 μM (\blacksquare), 3.5 μM (\blacktriangle), 5 μM (\blacktriangledown)].

Table 6. Summary of MtSDH inhibition.

Compound	IC ₅₀ (μ M)	3DHS titration			NADPH titration		
		Inhibition mode	K_i (μ M)	αK_i (μ M)	Inhibition mode	K_i (μ M)	αK_i (μ M)
2	3.2 \pm 0.4	mixed	3.1 \pm 0.5	8.7 \pm 0.3	non-competitive	8.5 \pm 1.4	-
5	3.0 \pm 0.2	non-competitive	8.6 \pm 1.0	-	non-competitive	5.2 \pm 0.8	-
6	4.6 \pm 0.3	non-competitive	8.9 \pm 1.4	-	mixed	2.2 \pm 0.3	15.9 \pm 0.8
8	3.9 \pm 0.4	non-competitive	7.5 \pm 0.9	-	non-competitive	7.1 \pm 1.4	-
11	2.8 \pm 0.1	mixed	2.9 \pm 0.9	5.3 \pm 0.8	non-competitive	4.0 \pm 0.5	-

The data collected for titration of 3DHS and NADPH at different inhibitor concentrations were plotted as double-reciprocal plots displaying a series of intersecting lines (Figures 8 and 9). The kinetic data was fit to four possible modes of inhibition: competitive, noncompetitive, uncompetitive and mixed inhibition. The inhibition constants for the inhibitors were determined from the best fitting mode, summarized in Table 6. All the selected inhibitors showed best fit to non-competitive or mixed mode of inhibition and in both types of inhibition, the inhibitor is able to bind to free enzyme, forming enzyme-inhibitor (EI) complex, as well as the substrate bound enzyme, forming enzyme-substrate-inhibitor (ESI) complex. The inhibition constant, K_i , in a non-competitive mode refers to the overall affinity of the inhibitor to free enzyme and enzyme-substrate complex. The mixed type of inhibition is a sub-type of non-competitive inhibition, where inhibition constants, K_i and αK_i , refer to the affinity of inhibitor to free enzyme and enzyme-substrate complex, respectively. When the value of α is greater than 1, the inhibitor has higher affinity to free enzyme, forming EI complex, than substrate bound enzyme, forming ESI complex.

Kinetic analysis indicates that compounds **5**, **6** and **8** are non-competitive inhibitors, whereas compounds **2** and **11** are mixed-type inhibitors with respect to 3DHS. Compound **2**, 5-chloro-7-(morpholino(thiophen-2-yl)methyl)quinolin-8-ol and compound **11** containing naphthalene sulfonamide with thiazole subunit exhibited good potency with K_i of $3.1 \pm 0.5 \mu\text{M}$ and $2.9 \pm 0.9 \mu\text{M}$ and αK_i of $8.7 \pm 0.3 \mu\text{M}$ and $5.3 \pm 0.8 \mu\text{M}$, respectively. In the presence of 3DHS, the affinity to form ESI complex decreased more for compound **2** compared to compound **11**. On the other hand, compounds **2**, **5**, **8** and

11 are non-competitive inhibitors, whereas compound **6** is a mixed-type inhibitor with respect to NADPH. Compound **6** containing trifluoromethyl phenyl subunit was most potent with K_i of $2.2 \pm 0.3 \mu\text{M}$ and in the presence of NADPH the affinity, αK_i increased to $15.9 \pm 0.8 \mu\text{M}$. As shown in Table 1, these inhibitors exhibit different chemical scaffolds that can be modified for development of more potent inhibitors against MtSDH.

4. SUMMARY AND CONCLUSION

Mtb is the etiological agent of tuberculosis disease and is on the verge of becoming a formidable health threat, due to emergence of single-drug resistant, multiple-drug resistant and extensive-drug resistant strains against the first-line drugs, which have been in use since 1940s. Therefore, discovery of new antimycobacterial agents is imperative to counter re-emergence of tuberculosis. The availability of *Mtb* genomic information has enabled identification, testing and validation of molecular targets and pathways, suitable for inhibitor discovery and drug development.

Shikimate pathway plays a central role by linking carbohydrate metabolism to biosynthesis of aromatic compounds in bacteria, fungi, plants and apicomplexan parasites. In *Mtb*, the genes involved in this pathway are shown to be essential for bacterial cell viability. SDH is the fourth enzyme of shikimate pathway catalyzing the reversible conversion of 3DHS to SKM utilizing NADP(H) cofactor. MtSDH is reported to stereo-specifically transfer C4-*proS* hydride of NADP(H) suggesting that the cofactor binds to enzyme in *syn* conformation, as opposed to well characterized homologs of SDH, which are known to stereo-specifically transfer C4-*proR* hydride while NADP(H) binds to enzyme in *anti* conformation. The molecular/structural basis of this difference has implications in development of MtSDH specific inhibitors and is not known due to lack of three dimensional structural analysis of MtSDH.

In this study, the crystal structure of MtSDH was determined in the apo-form and in complex with SKM. The overall structure of MtSDH is modular; composed of N-

terminal substrate binding domain with α/β architecture and C-terminal cofactor binding domain with Rossmann fold. The two modules are interconnected by two helices forming an active site groove where catalysis occurs. The structural variation in different crystal forms of MtSDH reported here, allowed the identification of hinge region located between the two structural modules in $\alpha 5$ and $\alpha 13$ helices and plays a significant role in open and closed conformation of the enzyme, which is linked to its activity. Structural comparison with SDH homologs reveal that in MtSDH a series of helices, $\alpha 9$, $\eta 10$ and $\alpha 11$ connecting $\beta 10$ and $\beta 11$ strands replace a long loop and this region may undergo structural changes upon cofactor binding. Based on the MtSDH-shikimate complex structure, NADP^+ was modeled reliably in the cofactor binding site. The analysis reveals that in addition to residues in “basic patch”, Ser125 within the glycine rich loop may interact with the 2'-phosphate of adenine ribose and form a novel cofactor binding microenvironment in SDH family of enzymes. Based on the model, it is clear that specific interactions between MtSDH and amide group of NADP(H)'s nicotinamide ring confers cofactor binding in *anti* conformation, which will result in stereospecific transfer of C4-*proR* hydride of NADPH as opposed to C4-*proS* hydride transfer as reported earlier.

Biochemically, five inhibitors of MtSDH identified previously from a high-throughput enzyme assay screen were characterized. The dose-dependent inhibition showed IC_{50} values of these compounds range from 2.8-4.6 μM . Inhibition mode was investigated and all the compounds displayed non-competitive or mixed inhibition mode with respect to substrate and cofactor. Compound **6**, 2-(1H-benzo[d]imidazol-2(3H)-

ylidene)-3-oxo-4-(5-(3-(trifluoromethyl)phenyl)-2*H*-tetrazol-2-yl)butanenitrile was most potent with K_i of $2.2 \pm 0.3 \mu\text{M}$. Compound **2**, 5-chloro-7-(morpholino(thiophen-2-yl)methyl)quinolin-8-ol and compound **11**, 2-(1,1-dioxido-2*H*-naphtho[1,8-*cd*]isothiazol-2-yl)-*N*-(5-methylthiazol-2-yl)acetamide also exhibited good potency with K_i of $3.1 \pm 0.5 \mu\text{M}$ and $2.9 \pm 0.9 \mu\text{M}$.

This study is the first report of MtSDH crystal structure elucidating structural features to gain insight into specific interactions of enzyme with substrate and cofactor. The characterization of MtSDH inhibitors containing different chemical scaffolds along with the crystal structure lays the foundation for structure-guided design and development of MtSDH specific inhibitors with increased activity.

REFERENCES

1. World Health Organization. (2009) *Global tuberculosis control : epidemiology, strategy, financing : WHO report 2009*, World Health Organization, Geneva.
2. Jassal, M., and Bishai, W. R. (2009) Extensively drug-resistant tuberculosis, *Lancet Infect Dis* 9, 19-30.
3. Cole, S. T., Brosch, R., Parkhill, J., Garnier, T., Churcher, C., Harris, D., Gordon, S. V., Eiglmeier, K., Gas, S., Barry, C. E., 3rd, Tekaia, F., Badcock, K., Basham, D., Brown, D., Chillingworth, T., Connor, R., Davies, R., Devlin, K., Feltwell, T., Gentles, S., Hamlin, N., Holroyd, S., Hornsby, T., Jagels, K., Krogh, A., McLean, J., Moule, S., Murphy, L., Oliver, K., Osborne, J., Quail, M. A., Rajandream, M. A., Rogers, J., Rutter, S., Seeger, K., Skelton, J., Squares, R., Squares, S., Sulston, J. E., Taylor, K., Whitehead, S., and Barrell, B. G. (1998) Deciphering the biology of *Mycobacterium tuberculosis* from the complete genome sequence, *Nature* 393, 537-544.
4. Herrmann, K. M., and Weaver, L. M. (1999) The shikimate pathway, *Annu Rev Plant Physiol Plant Mol Biol* 50, 473-503.
5. Roberts, F., Roberts, C. W., Johnson, J. J., Kyle, D. E., Krell, T., Coggins, J. R., Coombs, G. H., Milhous, W. K., Tzipori, S., Ferguson, D. J., Chakrabarti, D., and McLeod, R. (1998) Evidence for the shikimate pathway in apicomplexan parasites, *Nature* 393, 801-805.
6. Steinrucken, H. C., and Amrhein, N. (1980) The herbicide glyphosate is a potent inhibitor of 5-enolpyruvyl-shikimic acid-3-phosphate synthase, *Biochem Biophys Res Commun* 94, 1207-1212.
7. Schonbrunn, E., Eschenburg, S., Shuttleworth, W. A., Schloss, J. V., Amrhein, N., Evans, J. N., and Kabsch, W. (2001) Interaction of the herbicide glyphosate with its target enzyme 5-enolpyruvylshikimate 3-phosphate synthase in atomic detail, *Proc Natl Acad Sci U S A* 98, 1376-1380.
8. Parish, T., and Stoker, N. G. (2002) The common aromatic amino acid biosynthesis pathway is essential in *Mycobacterium tuberculosis*, *Microbiology* 148, 3069-3077.
9. Duncan, K., Edwards, R. M., and Coggins, J. R. (1987) The pentafunctional arom enzyme of *Saccharomyces cerevisiae* is a mosaic of monofunctional domains, *Biochem J* 246, 375-386.

10. Hawkins, A. R., and Smith, M. (1991) Domain structure and interaction within the pentafunctional arom polypeptide, *Eur J Biochem* 196, 717-724.
11. Bonner, C. A., and Jensen, R. A. (1994) Cloning of cDNA encoding the bifunctional dehydroquinase.shikimate dehydrogenase of aromatic-amino-acid biosynthesis in *Nicotiana tabacum*, *Biochem J* 302 (Pt 1), 11-14.
12. Deka, R. K., Anton, I. A., Dunbar, B., and Coggins, J. R. (1994) The characterisation of the shikimate pathway enzyme dehydroquinase from *Pisum sativum*, *FEBS Lett* 349, 397-402.
13. Pittard, J., and Wallace, B. J. (1966) Distribution and function of genes concerned with aromatic biosynthesis in *Escherichia coli*, *J Bacteriol* 91, 1494-1508.
14. Herrmann, K. M. (1995) The shikimate pathway: Early steps in the biosynthesis of aromatic compounds, *Plant Cell* 7, 907-919.
15. Michel, G., Roszak, A. W., Sauve, V., Maclean, J., Matte, A., Coggins, J. R., Cygler, M., and Laphorn, A. J. (2003) Structures of shikimate dehydrogenase AroE and its Paralog YdiB. A common structural framework for different activities, *J Biol Chem* 278, 19463-19472.
16. Giles, N. H., Case, M. E., Baum, J., Geever, R., Huiet, L., Patel, V., and Tyler, B. (1985) Gene organization and regulation in the qa (quinic acid) gene cluster of *Neurospora crassa*, *Microbiol Rev* 49, 338-358.
17. Wheeler, K. A., Lamb, H. K., and Hawkins, A. R. (1996) Control of metabolic flux through the quinate pathway in *Aspergillus nidulans*, *Biochem J* 315 (Pt 1), 195-205.
18. Singh, S., Korolev, S., Koroleva, O., Zarembinski, T., Collart, F., Joachimiak, A., and Christendat, D. (2005) Crystal structure of a novel shikimate dehydrogenase from *Haemophilus influenzae*, *J Biol Chem* 280, 17101-17108.
19. Peek, J., Lee, J., Hu, S., Senisterra, G., and Christendat, D. (2011) Structural and mechanistic analysis of a novel class of shikimate dehydrogenases: evidence for a conserved catalytic mechanism in the shikimate dehydrogenase family, *Biochemistry* 50, 8616-8627.
20. Peek, J., Garcia, C., Lee, J., and Christendat, D. (2013) Insights into the function of RifI2: structural and biochemical investigation of a new shikimate dehydrogenase family protein, *Biochim Biophys Acta* 1834, 516-523.

21. Fonseca, I. O., Silva, R. G., Fernandes, C. L., de Souza, O. N., Basso, L. A., and Santos, D. S. (2007) Kinetic and chemical mechanisms of shikimate dehydrogenase from *Mycobacterium tuberculosis*, *Arch Biochem Biophys* 457, 123-133.
22. Dansette, P., and Azerad, R. (1974) The shikimate pathway : II. Stereospecificity of hydrogen transfer catalyzed by NADPH-dehydroshikimate reductase of *E. coli*, *Biochimie* 56, 751-755.
23. Berman, H. M., Westbrook, J., Feng, Z., Gilliland, G., Bhat, T. N., Weissig, H., Shindyalov, I. N., and Bourne, P. E. (2000) The protein data bank, *Nucleic Acids Res* 28, 235-242.
24. Han, C., Hu, T., Wu, D., Qu, S., Zhou, J., Ding, J., Shen, X., Qu, D., and Jiang, H. (2009) X-ray crystallographic and enzymatic analyses of shikimate dehydrogenase from *Staphylococcus epidermidis*, *FEBS J* 276, 1125-1139.
25. Gan, J., Wu, Y., Prabakaran, P., Gu, Y., Li, Y., Andrykovitch, M., Liu, H., Gong, Y., Yan, H., and Ji, X. (2007) Structural and biochemical analyses of shikimate dehydrogenase AroE from *Aquifex aeolicus*: implications for the catalytic mechanism, *Biochemistry* 46, 9513-9522.
26. Bagautdinov, B., and Kunishima, N. (2007) Crystal structures of shikimate dehydrogenase AroE from *Thermus thermophilus* HB8 and its cofactor and substrate complexes: insights into the enzymatic mechanism, *J Mol Biol* 373, 424-438.
27. Otwinowski, Z., and Minor, W. (1997) Processing of X-ray diffraction data collected in oscillation mode, *Method Enzymol* 276, 307-326.
28. Adams, P. D., Afonine, P. V., Bunkoczi, G., Chen, V. B., Davis, I. W., Echols, N., Headd, J. J., Hung, L. W., Kapral, G. J., Grosse-Kunstleve, R. W., McCoy, A. J., Moriarty, N. W., Oeffner, R., Read, R. J., Richardson, D. C., Richardson, J. S., Terwilliger, T. C., and Zwart, P. H. (2010) PHENIX: a comprehensive Python-based system for macromolecular structure solution, *Acta Crystallogr D Biol Crystallogr* 66, 213-221.
29. Emsley, P., Lohkamp, B., Scott, W. G., and Cowtan, K. (2010) Features and development of Coot, *Acta Crystallogr D Biol Crystallogr* 66, 486-501.
30. Laskowski, R. A., Macarthur, M. W., Moss, D. S., and Thornton, J. M. (1993) Procheck - a program to check the stereochemical quality of protein structures, *J Appl Crystallogr* 26, 283-291.

31. Chen, V. B., Arendall, W. B., 3rd, Headd, J. J., Keedy, D. A., Immormino, R. M., Kapral, G. J., Murray, L. W., Richardson, J. S., and Richardson, D. C. (2010) MolProbity: all-atom structure validation for macromolecular crystallography, *Acta Crystallogr D Biol Crystallogr* 66, 12-21.
32. Pettersen, E. F., Goddard, T. D., Huang, C. C., Couch, G. S., Greenblatt, D. M., Meng, E. C., and Ferrin, T. E. (2004) UCSF Chimera--a visualization system for exploratory research and analysis, *J Comput Chem* 25, 1605-1612.
33. Singh, S. A., and Christendat, D. (2006) Structure of *Arabidopsis* dehydroquinate dehydratase-shikimate dehydrogenase and implications for metabolic channeling in the shikimate pathway, *Biochemistry* 45, 7787-7796.
34. Lindner, H. A., Nadeau, G., Matte, A., Michel, G., Menard, R., and Cygler, M. (2005) Site-directed mutagenesis of the active site region in the quinate/shikimate 5-dehydrogenase YdiB of *Escherichia coli*, *J Biol Chem* 280, 7162-7169.
35. Rodrigues, V. S., Jr., Breda, A., Santos, D. S., and Basso, L. A. (2009) The conserved Lysine69 residue plays a catalytic role in *Mycobacterium tuberculosis* shikimate dehydrogenase, *BMC Res Notes* 2, 227.
36. Thoden, J. B., Frey, P. A., and Holden, H. M. (1996) Crystal structures of the oxidized and reduced forms of UDP-galactose 4-epimerase isolated from *Escherichia coli*, *Biochemistry* 35, 2557-2566.
37. Thoden, J. B., Frey, P. A., and Holden, H. M. (1996) High-resolution X-ray structure of UDP-galactose 4-epimerase complexed with UDP-phenol, *Protein Sci* 5, 2149-2161.
38. Somers, W. S., Stahl, M. L., and Sullivan, F. X. (1998) GDP-fucose synthetase from *Escherichia coli*: structure of a unique member of the short-chain dehydrogenase/reductase family that catalyzes two distinct reactions at the same active site, *Structure* 6, 1601-1612.
39. Fonseca, I. O., Magalhaes, M. L., Oliveira, J. S., Silva, R. G., Mendes, M. A., Palma, M. S., Santos, D. S., and Basso, L. A. (2006) Functional shikimate dehydrogenase from *Mycobacterium tuberculosis* H37Rv: purification and characterization, *Protein Expr Purif* 46, 429-437.